EVALUATION OF PV INVERTER CONTROL SCHEMES UNDER DISTORTED AND VARIABLE FREQUENCY GRID CONDITIONS

Sotirios NANOU(1) Efstratios BATZELIS(1) Stavros PAPATHANASSIOU(1)

(1) NTUA, Electric Power Division, 9 Iroon Politechniou str., 15780, Athens, Greece

e-mail: st@power.ece.ntua.gr

ABSTRACT: In this paper, a PV inverter control scheme is presented suitable for operation under distorted and unbalanced grid voltage, as well as when the grid frequency varies, as is the case in isolated systems such as those in non-interconnected islands. The analysis is performed both in the frequency and time domains, using a suitable linearized model, as well as the full non-linear electrical model of the system. The objective is to determine the main factors affecting the system dynamic behavior as well as the power quality characteristics of the PV output current in presence of distorted grid conditions. To this end, a comparative assessment of the proposed PV inverter controller versus a conventional one is performed.
Keywords: DC-AC-Converter, Modelling, PV System, System Performance

1 INTRODUCTION

Present day technical guidelines for the connection of PV units to the grid mandate flexibility in operation and enhanced power quality characteristics. This in turn requires the development of sophisticated control schemes for PV inverters which are capable of handling non-ideal grid conditions.

Grid synchronization of power converters has been the subject of several publications, e.g. [1]-[3]. It is well-known that the response of a 3-phase phase locked loop (PLL) operating in the synchronous rotating frame (SRF) degrades seriously when the utility voltage is unbalanced or distorted. To deal with this, advanced PLL control strategies have been proposed, which provide immunity under distorted or unbalanced grid conditions, such as a synchronous rotating frame (SRF) PLL equipped with double second order generalized integrator (DSOGI) filters [1]. Further, advanced control schemes for harmonic compensation (HC) of the inverter current have been proposed in the relevant literature [4]-[6], such as the use of multiresonant PR regulators [6], in order to maintain low current Total Harmonic Distortion (THD) values even in the presence of distorted grid voltages.

The main focus of this paper is to illustrate the key factors affecting the performance of such control schemes when applied to large-scale PV inverters connected to the LV network. As the inverter rating increases, considerably lower switching frequencies are utilized, which inevitably lower the bandwidth of the inverter controller and its stability margins. Moreover, the LC output filters employed in PV inverters, along with the inductance of the network, particularly of the MV/LV transformer, may give rise to low frequency resonances which can further degrade the power quality characteristics of the inverter output current in the presence of distorted grid conditions, even when HC schemes are employed.

The electrical scheme of the simulated PV plant is described in Section 2. The control philosophy applied to the PV system along with the frequency domain analysis is discussed in Section 3. Time domain simulations are presented and discussed in Section 4 and the main conclusions are summarized in Section 5.

2 PV SYSTEM MODEL

In order to assess the performance of the PV inverter controller, the study case system shown in Fig. 1 has been used. It comprises a 100 kW PV generator controlled by a buck-boost DC/DC converter and a DC/AC converter connected to the grid via an output LC filter and a MV/LV transformer. A large non linear load is assumed to be connected at the MV side of the transformer to introduce voltage distortion.

The PV generator has been modeled by its single-diode equivalent circuit [7]. The DC/DC converter control scheme, which regulates the output PV voltage, is presented in detail in [8]. The PV inverter is a standard 3-phase 2-level DC/AC converter. The full non-linear PV system electrical model is implemented in MATLAB/SIMULINK.

Parameters for the PV system and the network are presented in Tables I and II respectively.

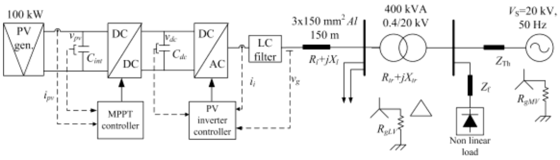

Figure 1: Two-stage PV power converter.

Table I: Parameters of the simulated system

Parameter	Symbol	Value
PV gen. MPP power (STC)	$P_{mpp,STC}$	100 kW
Intermediate capacitance	C_{int}	3 mF
DC/DC inductance	L_{dc}	20 mH
DC/DC capacitance	C_{dc}	10 mF
Rated DC link voltage	V_{dc}	700 V
LC Filter inductance	L_f	0.50 mH
LC Filter resistance	R_d	50 mΩ
LC filter capacitance	C_f	300 μF
DC/DC and DC/AC converter switching freq.	f_{sw}	2.5 kHz
Sampling & Transport delay	T_d	150 μs

Table II: Network characteristics

Parameter	Value
R_l+jX_l	0.264+j0.071 Ω/km
$R_{tr}+jX_{tr}$	1.15+j3.83 %
R_{gLV}, R_{gMV}	1 Ω
Z_{Th}	4∠65°

3 PV INVERTER CONTROLLER

The control scheme under study is depicted in Fig. 2. For grid synchronization, the PLL unit of Fig. 3(a) is employed, which comprises a conventional SRF-PLL equipped with a positive sequence extraction unit, based on adaptive DSOGI filters (Fig. 3(b)). The inverter controller, illustrated in Fig. 2, is based on an outer control loop which regulates the dc link voltage and an inner current control loop which regulates the inverter current [4]. To this end, a PR compensator with additional HC terms for selective harmonic compensation (3rd, 5th and 7th harmonics) is employed [6]. The PR regulator is frequency adaptive, utilizing the frequency provided by the PLL controller, ω_{pll}. The measured positive sequence voltage component is fed forward to the control loop of Fig. 2, accelerating the transient response of the system.

For tuning the current and DC voltage controllers, the system equations are linearized to derive open loop transfer functions. Standard frequency domain analysis techniques are then applied, with the objective of achieving a phase margin of at least 50 deg, while maintaining high gain crossover frequencies. In Fig. 4 the single phase representation of the control concept of Fig. 2 is shown in block diagram form. In order to simplify the control design analysis, the network inductance is represented by the transformer inductance L_{tr}. A time delay e^{-sT_d} has been included, which represents transport and sampling delays introduced by the inverter controller action [9], whereas the time constant T_f represents the lag introduced by antialising filters in current measurement [4].

As a general rule, the sampling frequency f_s is commonly chosen at twice the switching frequency [4], [9]. However, if the switching frequency is low, such as in the case of power converters of high rating, this selection could reduce notably the available bandwidth of the inverter controller. This is evident in Fig. 5, where the Bode plot of the open loop transfer function of the control loop of Fig. 4 is presented for two sampling rates. Here a sampling frequency of 10 kHz is assumed, which corresponds to a sampling and transport delay time constant of 150 μs (Table I) [9].

The HC terms shown in Fig. 2 are based on additional resonant controllers which compensate the specified current harmonics [6]. Based on the Bode plot of Fig. 5, which is reproduced in Fig. 6(a), it can be deduced that the gain crossover frequency of 479 Hz enables the use of HC terms for harmonics up to 7th, which don't affect significantly the stability margin of the PR controller.

A useful tool to evaluate the HC capability of the PR+HC controller is the harmonic impedance of the system Z_{in} which is expressed by [10]:

$$Z_{in} = \frac{v_s}{i_g} \qquad (1)$$

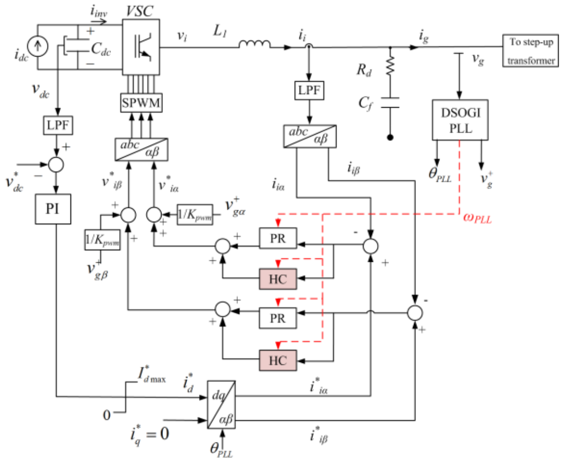

Figure 2: PV inverter control scheme.

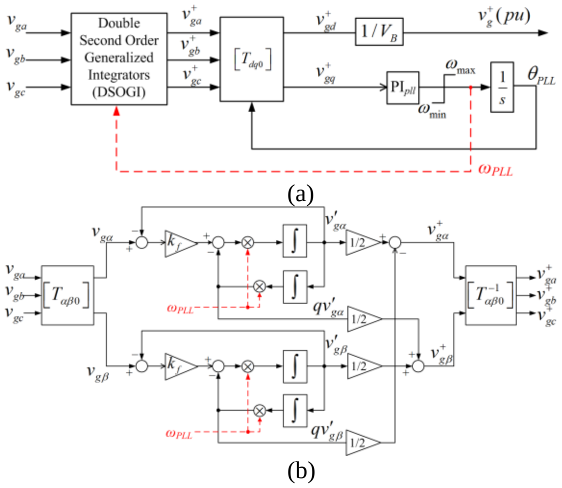

Figure 3: DSOGI-PLL: a) overall PLL structure, b) DSOGI filters.

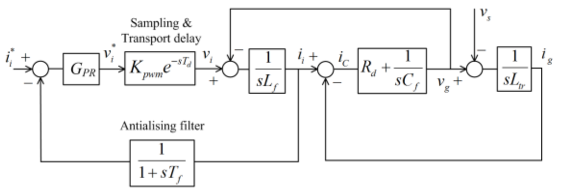

Figure 4: Block diagram of the current control scheme of Fig. 2.

In Fig. 6(b) the Bode plot of the harmonic impedance of the system is depicted, assuming a simple PR and a PR+HC controller. It is clear that the HC method increases the harmonic impedance at the 3rd, 5th and 7th harmonics, though the harmonic disturbance rejection capability gradually decreases. The impedance value reduces notably around the resonant frequency of the LC filter- network impedance, indicating that the presence of voltage harmonics in this range would amplify the inverter output current harmonics.

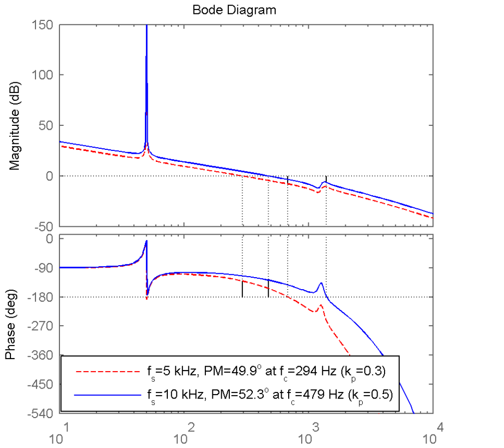

Figure 5: Bode plot of the open loop transfer function of the control loop of Fig. 4, for different sampling frequencies.

4 TIME DOMAIN RESPONSE

In this Section, time domain simulations are performed in order to evaluate the performance of the PV inverter controller of Fig. 2 and to verify the results obtained from the frequency domain analysis in the previous Section.

The satisfactory behavior of the DSOGI-PLL operating in a polluted and variable frequency grid is shown in Fig. 7, where its response is compared with that of a conventional SFR-PLL. During the time interval 0.5 – 1 s a transient increase of the frequency takes place, while at the same time it is assumed that the grid voltage becomes distorted (harmonic content as in Fig. 8(a)) and unbalanced (5% ratio of negative to positive sequence component). From Fig. 7 it is evident that the DSOGI-PLL provides a fairly accurate estimation of both the grid frequency and the positive sequence grid voltage, irrespective of the utility conditions. Hence, the estimate of the grid frequency can be reliably utilized, making the current regulator frequency adaptive, as depicted in Fig. 2.

In the following, the performance of the PR+HC controller is evaluated assuming different harmonic profiles of the grid voltage. In Fig. 8, the PV system response has been simulated under grid voltage distortion according to Fig. 8(a) and nominal grid frequency. From Fig. 8(c) it is clear that a drastic reduction in the harmonic content of the inverter-side current is achieved for harmonics up to 7^{th}, whereas the 11^{th} harmonic remains uncompensated since the available bandwidth of the control loop does not enable the use of higher frequency HC terms (based on Fig. 6(a)). This in turn reduces the THD of the inverter output current from 5.61% to 4.14%, as shown in Fig. 8(b).

The harmonic compensation capability of the PR+HC controller, demonstrated in Fig. 8(b), can be notably degraded if its resonance frequency is fixed and the grid frequency varies. This is evident in Fig. 9, where the harmonic content of the inverter side and grid side currents is shown when the grid frequency is 52 Hz. These results are obtained by simulation of the PV system response under the variable frequency conditions of Fig. 7(a). It is noteworthy that if a fixed frequency controller is assumed, the THD of the inverter output

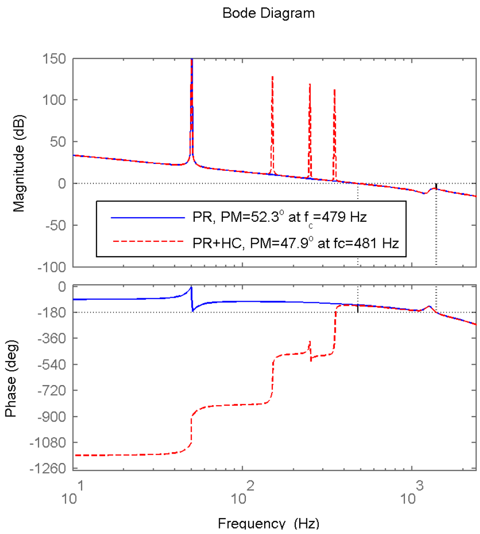

(a)

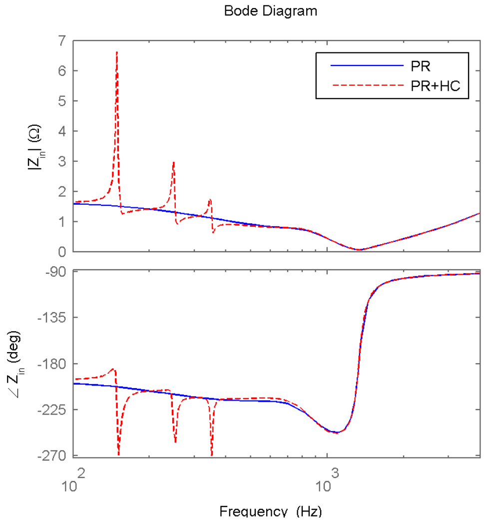

(b)

Figure 6: Bode plots of: a) open loop transfer function of the block diagram of Fig. 4, b) harmonic impedance Z_{in}.

current is notably higher from that of Fig. 8(b), as the addition of HC terms leads to a transient depression of the harmonic impedance Z_{in} at frequencies just above the resonant frequency of each HC term. This is clearly illustrated in Fig. 6(b) and demonstrates the necessity of employing a frequency adaptive concept for the PR+HC controller, which manages to reduce the THD of the inverter output current from 7.80% to 4.04% (Fig. 9(a)). However, it should be noted that the use of a conventional PR regulator doesn't compromise the accuracy of the dc link voltage control loop which remains effective, as the dc voltage controller compensates for the steady-state error of the PR regulator, readjusting the reference active current i_d^* (Fig. 10).

Another test of the PR+HC controller performance is conducted, assuming now a more extended harmonic spectrum for the grid voltage, generated by the nonlinear load shown in Fig. 1. The resulting harmonic content of the voltage at the MV side is shown in Fig. 11(a) and the spectrum of the inverter side and grid side currents in Figs. 11(b) and 11(c). The positive effect of the PR+HC

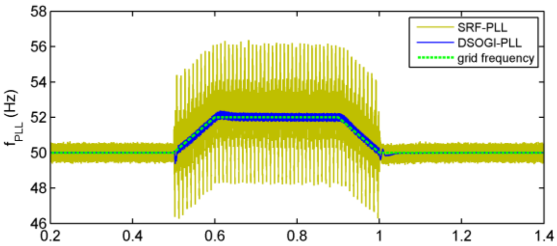

(a)

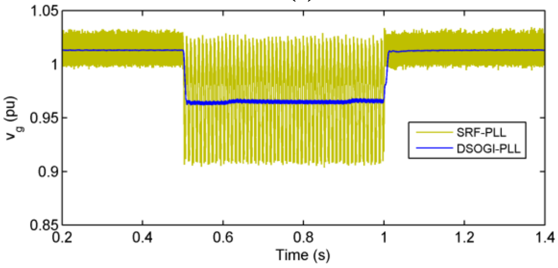

(b)

Figure 7: Response of the DSOGI-PLL and the conventional SFR-PLL during frequency deviations, under distorted and unbalanced grid voltages, a) frequency estimation, b) grid voltage estimation.

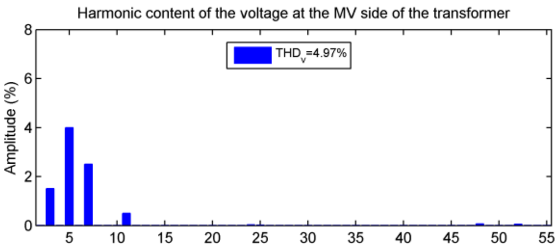

(a)

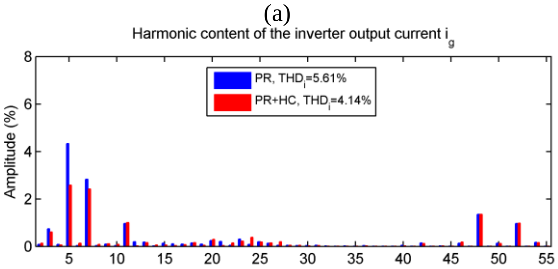

(b)

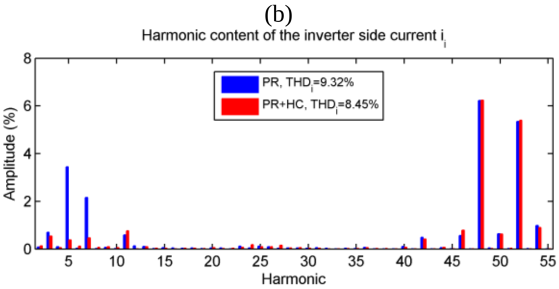

(c)

Figure 8: Performance of the inverter current regulator under polluted conditions. Harmonic content of a) the voltage at the MV side, b) the inverter output current, c) the inverter-side current.

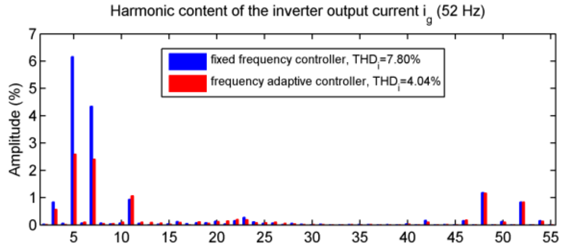

(a)

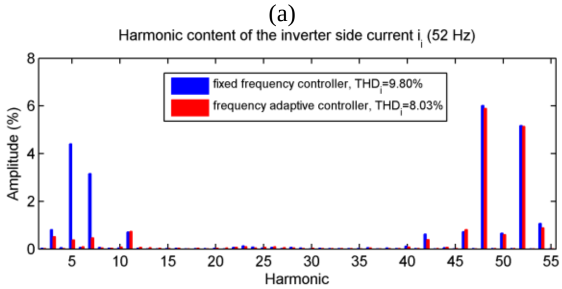

(b)

Figure 9: Harmonic content of a) the inverter output current, b) inverter-side current, at 52 Hz grid frequency (time interval 0.6 – 0.9 s in Fig. 7(a)).

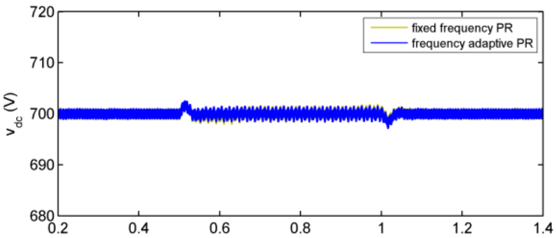

(a)

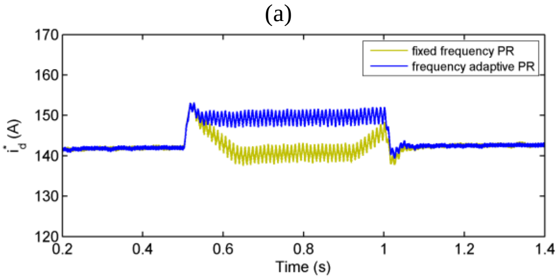

(b)

Figure 10: PV inverter controller response under the operating conditions of Fig. 7, a) DC link voltage controller, b) current controller.

regulator is clear in the low frequency range. At the same time, however, the notably higher distortion of the current is evident, compared to that of Fig. 8. This is attributed to the higher order harmonics, around the 25th order, which are amplified by the resonance between the LC output filter of the PV inverter and the MV/LV transformer, causing the large reduction in the harmonic impedance shown in Fig. 6(b). This result indicates that the performance of HC techniques similar to that presented in Fig. 2 could be inadequate in the presence of higher order voltage harmonics. Consequently, additional damping of the system should be investigated in such cases, such as employing active damping techniques [11].

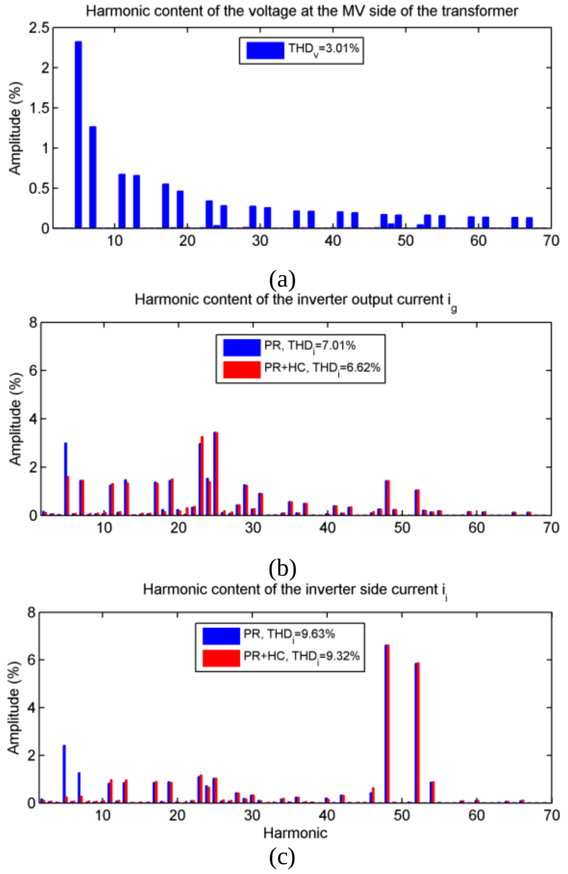

Figure 11: Performance of the inverter current regulator in the presence of a resonance between the inverter LC filter and the network inductance. Harmonic content of a) voltage at the MV side and b) the inverter output current, c) the inverter-side current.

5 CONCLUSION

In this paper, a PV inverter control scheme is developed for operation under polluted grid conditions and the compensator design is carried out. Criteria for the evaluation of the performance of the controller were the phase margin, the gain crossover frequency of the open loop transfer function of the system and the harmonic impedance of the system.

It has been shown that the stability margin of the system is strongly dependent on the sampling and transport delay of the inverter controller, which in turn influences the controller bandwidth and therefore the HC capability of the controller.

Results obtained from time domain simulations demonstrate that the DSOGI-PLL provides the required immunity under distorted and variable frequency grid conditions. Therefore, it can be reliably utilized in order to attain an optimum performance for the PV inverter controller.

Finally, it has been shown that the presented control scheme improves significantly the power quality characteristics of the inverter output current in the presence of low order voltage harmonics. However, additional control amendments could be necessary, apart from the HC techniques presented in this paper, in order to mitigate current harmonics in the presence of higher order voltage harmonics, due to the resonance between the LC output filter of the PV inverter and the inductance of the network.

6 REFERENCES

[1] A. Luna, C. Citro, C. Gavriluta, J. Hermoso, I. Candela, P. Rodriguez, “Advanced PLL structures for grid synchronization in distributed generation”, in *Proc. International Conference on Renewable Energies and Power Quality*, 2012.

[2] F. Gonzalez-Espin, E. Figueres, G. Garcera, “An Adaptive Synchronous-Reference-Frame Phase-Locked Loop for Power Quality Improvement in a Polluted Utility Grid”, *IEEE Trans. Industrial Electronics*, vol. 59, no. 6, June 2012.

[3] P. Rodriguez, A. Luna, R. Santiago, I. Etxaberria, R. Teodorescu, F. Blaabjerg, “A Stationary Reference Frame Grid Synchronization System for Three-Phase Grid-Connected Power Converters Under Adverse Grid Conditions”, *IEEE Trans. Power Electronics*, vol. 27, no. 1, Jan.2012.

[4] F. Gonzalez-Espin, G. Garcera, I. Patrao, E. Figueres, “An Adaptive Control System for Three-Phase Photovoltaic Inverters Working in a Polluted and Variable Frequency Electric Grid”, *IEEE Trans. Power Electronics*, vol. 27, no. 10, Oct. 2012.

[5] A. V. Timbus, M. Cioboratu, R. Teodorescu, “Adaptive Resonant Controller for Grid-Connected Converters in Distributed Power Generation Systems”, in *Proc. 21st Annual IEEE Applied Power Electronics Conference and Exposition*, 2006.

[6] R. Teodorescu, F. Blaabjerg, U. Borup, M. Liserre, “A New Control Structure for Grid-Connected LCL PV Inverters With Zero Steady-State Error and Selective Harmonic Compensation”, *in Proc. 19th Annual IEEE Applied Power Electronics Conference and Exposition*, 2004.

[7] Weidong Xiao, William G. Dunford, Antoine Capel, “A Novel Modeling Method for Photovoltaic Cells”, in *Proc. 35th Annual IEEE Power Electronics Specialists Conference*, June 2004.

[8] S. Nanou, S. Papathanassiou, G. Vokas, “Small Signal Analysis and Gain Scheduling Control of a Photovoltaic DC/DC Converter”, in *Proc. 27th European Photovoltaic Solar Energy Conference and Exhibition*, Sep. 2012.

[9] D. G. Holmes, T. A. Lipo, B. P. McGrath, W. Y. Kong, “Optimized Design of Stationary Frame Three Phase AC Current Regulators”, *IEEE Trans. Power Electronics*, vol. 24, no. 11, Nov. 2009.

[10] E. Twining, D. G. Holmes, “Grid Current Regulation of a Three-Phase Voltage Source Inverter With an LCL Input Filter”, *IEEE Trans. Power Electronics*, vol.18, no. 3, May 2003.

[11] J. Dannehl, M. Liserre, F. W. Fuchs, “Filter-Based Active Damping of Voltage Source Converters With LCL Filter”, *IEEE Trans. Industrial Electronics*, vol.58, no. 8, Aug. 2011.